



Silver stoichiometry engineering: an alternative way to improve energy storage density of AgNbO_3 -based antiferroelectric ceramics

Nengneng Luo^{1,2,a)}, Xinya Tang¹, Kai Han¹, Li Ma^{1,2}, Zhenpei Chen¹, Xiyong Chen¹, Qin Feng¹, Changzheng Hu³, Yuezhou Wei¹, Fujita Toyohisa^{1,a)}

¹Guangxi Key Laboratory of Processing for Non-Ferrous Metallic and Featured Materials, School of Resources, Environment and Materials, Guangxi University, Nanning 530004, China

²Center On Nanoenergy Research, School of Resources, Environment and Materials, Guangxi University, Nanning 530004, China

³Key Laboratory of New Processing Technology for Nonferrous Metal & Materials, Ministry of Education/Guangxi Key Laboratory of Optical and Electronic Materials and Devices, Guilin University of Technology, Guilin 541004, China

^{a)}Address all correspondence to these authors. e-mails: luonn1234@163.com; fujitatoyohisa@gxu.edu.cn

Received: 13 September 2020; accepted: 17 November 2020; published online: 7 January 2021

Lead-free dielectric capacitor with high energy storage density is in great demand, but with the challenge of limited energy storage density. In this work, $\text{Ag}(\text{Nb}_{0.85}\text{Ta}_{0.15})\text{O}_{3-x}$ wt% Ag_2O (ANTA x) lead-free ceramics with nonstoichiometric Ag_2O were fabricated, with the aim of improving energy storage density. The element concentration, phase structure, microstructure, dielectric property, and energy storage performance were investigated. Improved recoverable energy storage density (W_{rec}) of 4.8 J/cm³ were achieved for ANTA1 ceramics with 1 wt% Ag_2O in excess, demonstrating obvious improvement compared with the stoichiometric counterpart. In addition, the ANTA1 ceramics also exhibited highly stable energy storage performance in the temperature range from room temperature to 150 °C, with variations less than 4% and 5% for W_{rec} and energy storage efficiency, respectively. The good properties may be associated with the dismissing of various defects by adding excess Ag_2O . This work demonstrates that silver stoichiometry engineering is an effective method to improve energy storage properties of AgNbO_3 -based antiferroelectric ceramics.

Introduction

In recent years, new clean and renewable energy technologies are in great demand due to the growing energy market and environmental protection conscious. Dielectric capacitor is attracting global attention in various advanced pulsed power systems, such as power distribution, transportation, spacecraft, medical devices, and weapons. These applications are ascribed to their significant advantages of high power density, rapid charge/discharge capability, and superb cycle reliability, compared to traditional electro-chemical capacitors and batteries [1–4]. Nevertheless, the low energy storage capability extremely limits their practical application in these fields. This enforces the

great efforts to improve the energy storage density of dielectric capacitors. As the core of a dielectric capacitor, the dielectric material is considered to be one of the most important factors that affect the energy storage density, which is under intensive investigation. As a consequence, many kinds of dielectric material systems (such as linear dielectrics [5], relaxor/ferroelectrics [6] and antiferroelectrics [7, 8]) have been developed to meet the demand of the dielectric capacitors. In comparison with other materials systems, antiferroelectric (AFE) materials are superior in achieving high recoverable energy density (W_{rec}), due to their double polarization hysteresis loops, accompanying with high maximum polarization (P_{max}) and small remnant polarization (P_r). However, most of the high energy storage performance

AFE materials are lead-based systems, such as $(\text{Pb,L a})(\text{Zr,T i})\text{O}_3$ and $(\text{Pb,L a})(\text{Zr,S n,T i})\text{O}_3$, which generally possess large amount of lead over 60 wt% [9, 10]. The usage of lead may cause some environmental problems and human health hazards, putting forward the high expectation of discovering novel environmentally friendly lead-free AFE energy storage materials.

As a new alternative sort of lead-free antiferroelectric materials that is promising for dielectric capacitor applications, AgNbO_3 was under intensive investigation in recent years. In general, the AgNbO_3 ceramics can exhibit high W_{rec} with value in the range of 1.5–2.0 J/cm³ depending on the applied electric field, attributed to the double-like polarization–electric (P – E) hysteresis loops under electric field [11, 12]. However, the weak ferroelectricity in this system leads to high remnant polarization, low critical electric field for antiferroelectric–ferroelectric phase transition, and large hysteresis, which make it unfavorable for improving energy storage density. In order to further improve the energy storage density, composition modifications (such as doping) were commonly adopted. The mostly used dopants include divalent alkaline earth metal ions [8] and trivalent lanthanide ions in A-site [13], higher valence ions in B-site [14–16], and the A-/B-site co-doping ions [17, 18], with substitution position depending on the chemical properties of dopants. For example, the divalent Ca^{2+} ions tended to replace the Ag^+ in A-site in Ca^{2+} -doped AgNbO_3 ceramics, resulting in highly recoverable energy storage density (W_{rec}) of 3.55 J/cm³, about two times of the value of virgin ones [8]. The trivalent Sm^{3+} ions also tended to locate in A-site after doping in AgNbO_3 ceramics, which further increased the recoverable energy storage density to 5.2 J/cm³, accompanying with good energy storage efficiency (η) of 68% [13]. As for the B-site dopants, the recoverable energy storage density of W^{6+} ions-doped AgNbO_3 ceramics was improved to be 3.3 J/cm³ [14], which reached 4.2 J/cm³ [15] and 6.3 J/cm³ [16] in Ta^{5+} ions-modified AgNbO_3 ceramics. In addition, the $\text{Sm}^{3+}/\text{Ta}^{5+}$ ions co-doped AgNbO_3 ceramics also showed high recoverable energy storage density of 4.87 J/cm³ [17]. This was also the case for $\text{Bi}(\text{Zn}_{2/3}\text{Nb}_{1/3})\text{O}_3$ -modified AgNbO_3 ceramics, in which high recoverable energy storage density of 4.6 J cm⁻³ was achieved [18]. In principle, one of the most important effect of the aforementioned dopants is to stabilize the antiferroelectricity by decreasing the tolerance factor or reducing the polarizability.

Actually, besides the above-mentioned methods, stoichiometry engineering is also considered as an effective way to optimize the physical properties of dielectric materials, especially for the systems with volatile elements. For example, in $\text{K}_x\text{Na}_{1-x}\text{NbO}_3$ -based piezoelectric materials, extra alkali carbonates in starting powders were suggested to be used to prevent the loss of alkali metal elements, thus improving the piezoelectric/ferroelectric properties [19, 20]. This method also exhibited advantage in Pb-based electroceramics, in

which excess lead oxide was usually added to compensate the loss of lead [21–23]. The addition of extra raw material was more commonly used when preparing film with volatile elements, where more than 10% excess volatile elements were added [24]. In AgNbO_3 system, the Ag_2O inevitably decomposes into Ag metal and O_2 gas in air at elevated temperature, which also leads to the volatilization of Ag metal during the sintering process [25, 26]. The loss of silver will cause the deviation of chemical composition from their nominal stoichiometric ratio and lead to Ag-deficient AgNbO_3 . As a result, silver vacancies (V'_{Ag}) are generally produced, so as the oxygen vacancies ($V_{\ddot{\text{O}}}$) to keep valance balance. Moreover, the $[2V'_{\text{Ag}} + V_{\ddot{\text{O}}}]^x$ complexes may also form on this occasion. First principle calculation revealed that the $[2V'_{\text{Ag}} + V_{\ddot{\text{O}}}]^x$ complexes in an antiferroelectric Pbcm matrix could act as the origin of the weak ferroelectricity in AgNbO_3 [27]. Therefore, the antiferroelectric characteristic may be weakened for the AgNbO_3 -based ceramics with Ag deficiency, which in turn increases remnant polarization and hysteresis, thus decaying the energy storage properties. Therefore, it's of great importance to understand the effect of nonstoichiometric Ag_2O on the physical properties of AgNbO_3 -based materials.

Based on the aforementioned considerations, nonstoichiometric Ag_2O were added in AgNbO_3 -based ceramics to look into the effect of silver deficiency and excess on the phase structure, microstructure, and electrical properties. As a promising lead-free antiferroelectric material, the stoichiometric $\text{Ag}(\text{Nb}_{0.85}\text{Ta}_{0.15})\text{O}_3$ ceramic exhibited stable antiferroelectric characteristic with ultrahigh recoverable energy storage density and efficiency [15]. Therefore, in this work, the $\text{Ag}(\text{Nb}_{0.85}\text{Ta}_{0.15})\text{O}_3$ - x wt% Ag_2O (ANTAx) lead-free ceramics with nonstoichiometric Ag_2O were selected as prototypes. Improved W_{rec} with value of 4.8 J/cm³ was achieved for ANTA1 ceramic with 1 wt% Ag_2O in excess, which also exhibited highly stable energy storage performance. This work paves a new way to improve the energy storage performance of AgNbO_3 -based antiferroelectric ceramics.

Results and discussion

Element concentration

Figure 1 gives the real element ratio of Ag, Nb, and Ta for the ANTA x ceramics with various Ag content detected by ICP measurement. As expected, the amount of Nb and Ta are almost the same with the nominal content, while the amount of Ag element is around 99.3% of the nominal value for the stoichiometric composition with $x = 0$ wt%, demonstrating around 0.7% Ag deficiency. The loss of Ag can be compensated only when more than 0.5 wt% excess Ag_2O is added,

because the measured real element ratios of Ag are 99.9% and 100.3% for samples with 0.5 and 1 wt% Ag_2O in excess, respectively. This indicates that a small part of silver is indeed lost during the sintering process. It should be noted that both metal Ag (if it exists in our case) and lattice Ag^+ are included in ICP measurement. Therefore, the lattice Ag^+ may be less than the measured value, even though no detectable silver metal is observed in this work (See the XRD result below).

Phase and microstructure

To investigate the effect of the silver deficiency and excess on phase structure evolution, XRD of the as-prepared samples are measured and shown in Fig. 2a. All samples exhibit similar XRD diffraction patterns, all of which can be well indexed without detectable extra peaks and peak split/shift for all samples. This indicates that a small amount of nonstoichiometric Ag_2O can neither introduce second phase (such as metallic silver or other metallic oxide) nor change the phase structure. It should be noted that changes are observed in the refined lattice parameters and cell volume for the ceramics with various Ag_2O content. The lattice parameters a and c stay relatively stable at lower Ag_2O content, which exhibit large enhancement at $x = 0.25$ wt%, as shown in Fig. 2b. The similar phenomenon can be also observed for the cell volume in Fig. 2c. These may be resulted from the decreased amount of silver vacancy and oxygen vacancy after the supplement of extra Ag_2O . Figure 2d–f gives the microstructure of the selected ceramics with various Ag_2O content of –1 wt%, 0 wt%, and 1 wt%, after polishing and hot corrosion. All samples exhibit closely compacted grains, indicating high relative density. It should be noted that the micromorphology and grain size are similar for the samples with various Ag_2O content, exhibiting polygonal shape with grain size distribution in the range from ~ 2 to ~ 5 μm , which indicates that a very small amount of Ag_2O deficiency or excess plays little effect on the microstructure.

Dielectric properties and energy storage performance

In order to find the evolution of dielectric property as a function of Ag_2O , temperature dependence of dielectric permittivity and loss are also measured, as given in Fig. 3a and b. Four dielectric anomalies associated with various phase transitions are observed for ANTAX ceramics in the temperature-dependent dielectric permittivity, as marked in Fig. 3a, consistent with the results reported in the literature [28]. The dielectric anomaly at ~ 200 °C is associated with the M2–M3 phase transition temperature. The two dielectric anomalies at ~ 346 °C and ~ 390 °C are related to the M3–O and O–T phase transitions, respectively. The small hump around 80 °C is assigned to be freezing temperature (T_f),

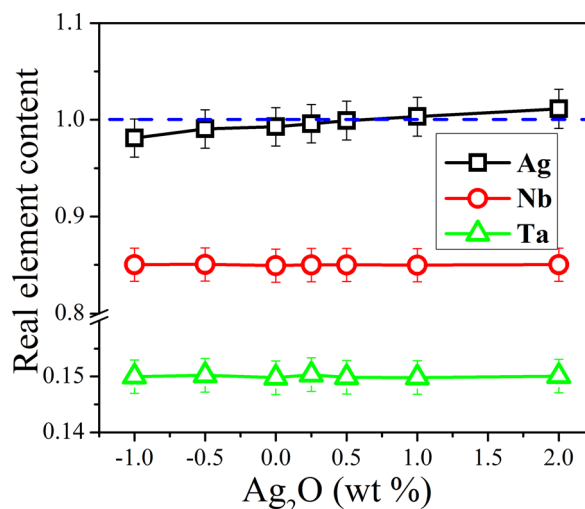


Figure 1: The real element ratio of Ag, Nb, and Ta for ANTAX ceramics with various Ag_2O content.

below which the antipolar B-site ions displacements are frozen, resulting in antiferroelectric ordering [29]. The dielectric anomaly related to M1–M2 phase transition is shifted to below room temperature in the ANTAX ceramics, which is invisible in the measuring temperature range. It should be noticed that all dielectric anomalies occur at the same temperature with the variation of Ag_2O content, which further demonstrates that the influence of silver deficiency and excess on the phase structure is very small. The dielectric permittivity gradually shifts to lower value with the excess of silver which is even more obvious at elevated temperature. This may be associated with the vanishing of defects mentioned before. In addition, all of the dielectric loss stays at low value for all samples, indicating high electrical resistivity.

Figure 4 gives the compositional dependence of antiferroelectric properties for the as-prepared ANTAX ceramics. Typical double P – E loops with low remnant polarization are observed for all of the as-prepared samples (Fig. 4a), indicating that all of the samples with silver deficiency and excess are well-stabilized antiferroelectrics. Four typical peaks are found in the I – E curves for all samples, with two peaks in the branch with positive electric field and the other two peaks with negative electric field, as shown in Fig. 4b, resulting from the reversible electric field-induced phase transitions. This further verifies that all of the samples are of antiferroelectrics. The peak at higher electric field in each branch is associated with the electric field-induced antiferroelectric to ferroelectric phase transition (the corresponding electric field is E_F), while the peak located at lower electric field is associated with the ferroelectric backward antiferroelectric phase transition (the corresponding electric field is E_A). To look insight into the effect of silver condition on the antiferroelectric property, the

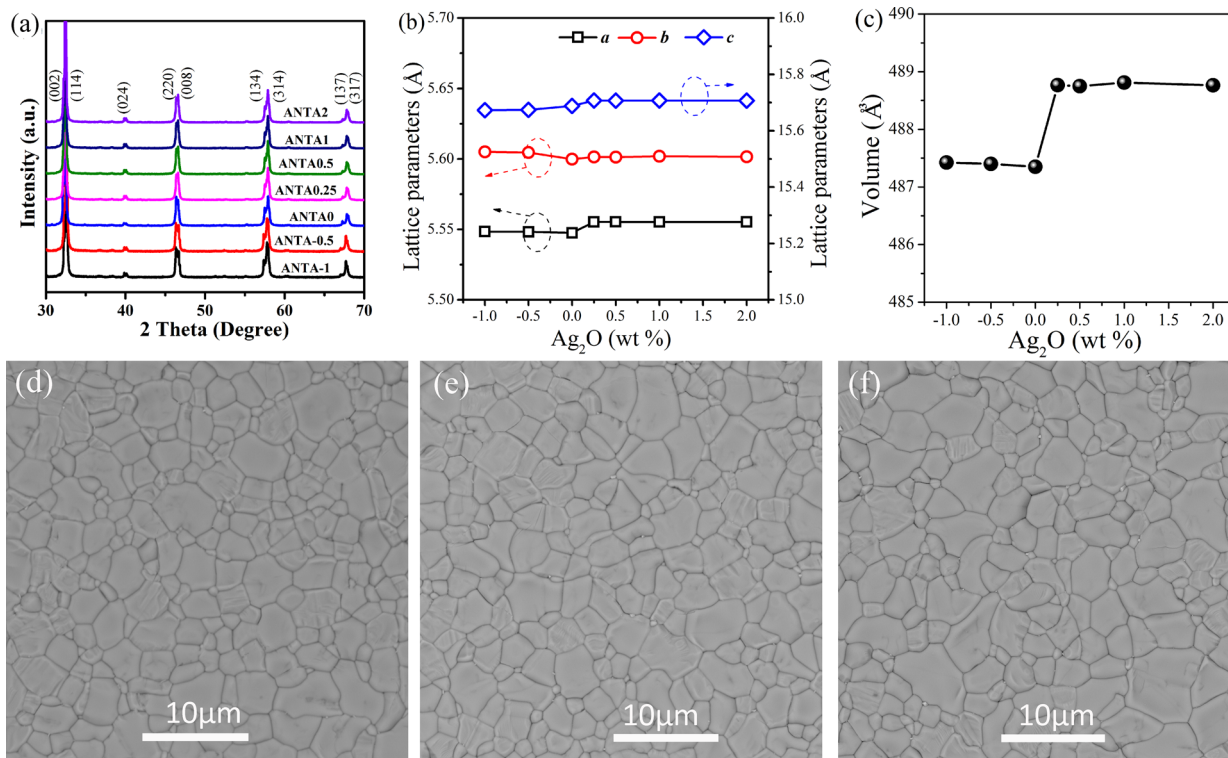


Figure 2: (a) The XRD patterns of the ANTA_x ceramics, (b) the calculated lattice parameters *a*, *b* and *c*, and (c) the cell volume. SEM micrographs of the selected ANTA_x ceramics with composition of (d) *x* = -1, (e) *x* = 0, and (f) *x* = 1.

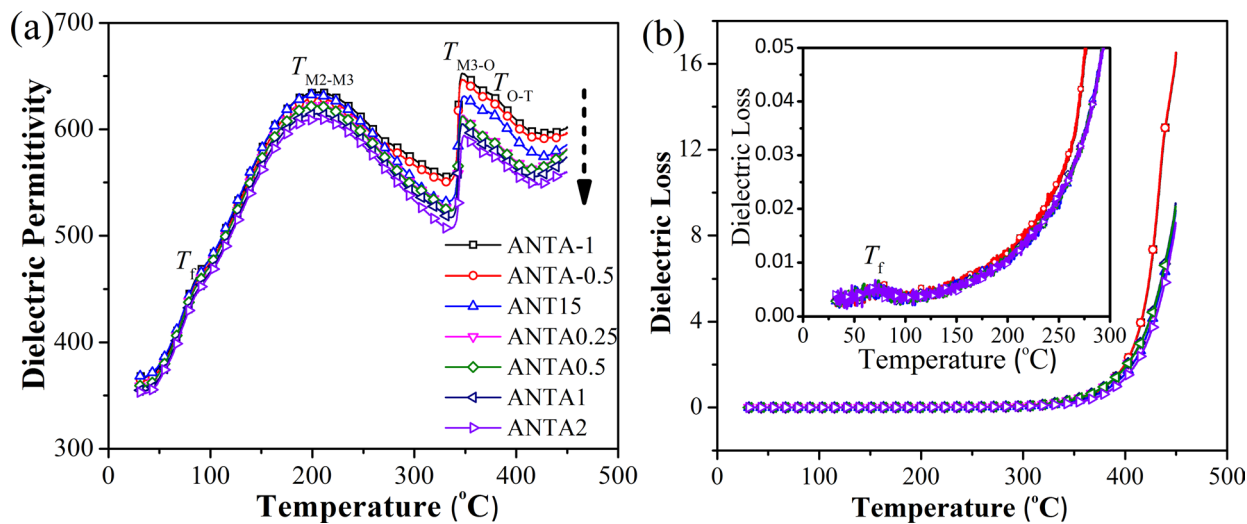


Figure 3: Temperature dependence of (a) dielectric permittivity and (b) loss of the as-prepared ANTA_x ceramics with various Ag₂O content.

Ag₂O-dependent polarization and critical electric field for phase transition are determined, respectively, from the *P*-*E* loops and *I*-*V* curves, as given in Fig. 4c and d. The maximum polarization exhibits a general increase with the increase of Ag₂O content, with a small kinking around *x* = 0.5 wt%, above which a relatively stable *P*_{max} is observed by further increasing

the Ag₂O content. In comparison, the *P*_r stays relatively stable across the whole Ag₂O content. The *E*_A and *E*_F also exhibit slight enhancement when the excess content of Ag₂O is lower than 0.5 wt%, similar to that observed in *P*_{max}. The evolution of remnant polarization and critical electric field for phase transition may indicate a possible enhancement in the stability

of antiferroelectric feature. As previously demonstrated, the ANTAx ceramics keep the same phase structure and phase transition temperature, which may result to a similar AFE characteristic. The improved stability of AFE feature in this work might be ascribed to the dismissal of various defects. The excess of silver may compensate the lost silver ions in the lattice due to the evaporation and decomposition of Ag_2O during sintering process. This will forbid the formation of silver vacancies, oxygen vacancies, as well as the $[2V'_{\text{Ag}} + V_{\text{O}}]^\times$ complexes, which are usually considered as the origin of the weak ferroelectricity in AgNbO_3 [27]. The similar mechanism may be also applicable in Ta-modified AgNbO_3 system, thus leading to improved stability of antiferroelectricity. A higher stability of antiferroelectricity may benefit the improvement of energy storage density.

Besides the antiferroelectric feature, the breakdown strength (E_b) is another crucial parameter that affects the energy storage performance. To understand the effect of Ag_2O efficiency and deficiency on the breakdown strength, E_b of the as-prepared samples with various Ag_2O content are evaluated according to the Weibull distribution [15]:

$$X_i = \ln(E_i) \quad (1)$$

$$Y_i = \ln\left(\ln\frac{1}{1 - N_i}\right) \quad (2)$$

$$N_i = \frac{i}{n + 1} \quad (3)$$

where n is the total number of samples, E_i is the breakdown electric field for the i th specimen, and N_i is the probability of dielectric breakdown. Good linear relationship is obtained for X_i and Y_i , as shown in Fig. 5a. The determined E_b as a function of Ag_2O content is given in Fig. 5b. Of great importance is that significant enhancement in E_b is observed for ceramics with the Ag_2O content increasing from -1 to 2 wt%, which changes from 225 to 276 kV/cm. The improvement in breakdown strength may be associated with the decreased amount of defects (such as silver vacancy, oxygen vacancy, and their complex, etc.) after the addition of extra Ag_2O . A higher breakdown strength is beneficial for improving energy storage density.

In General, the energy storage performance of a dielectric capacitor can be evaluated using the mathematical formulas as follows [17]:

The energy storage density:

$$W = \int_0^{P_{\max}} EdP \quad (4)$$

The recoverable energy storage density:

$$W_{\text{rec}} = \int_{P_r}^{P_{\max}} EdP \quad (5)$$

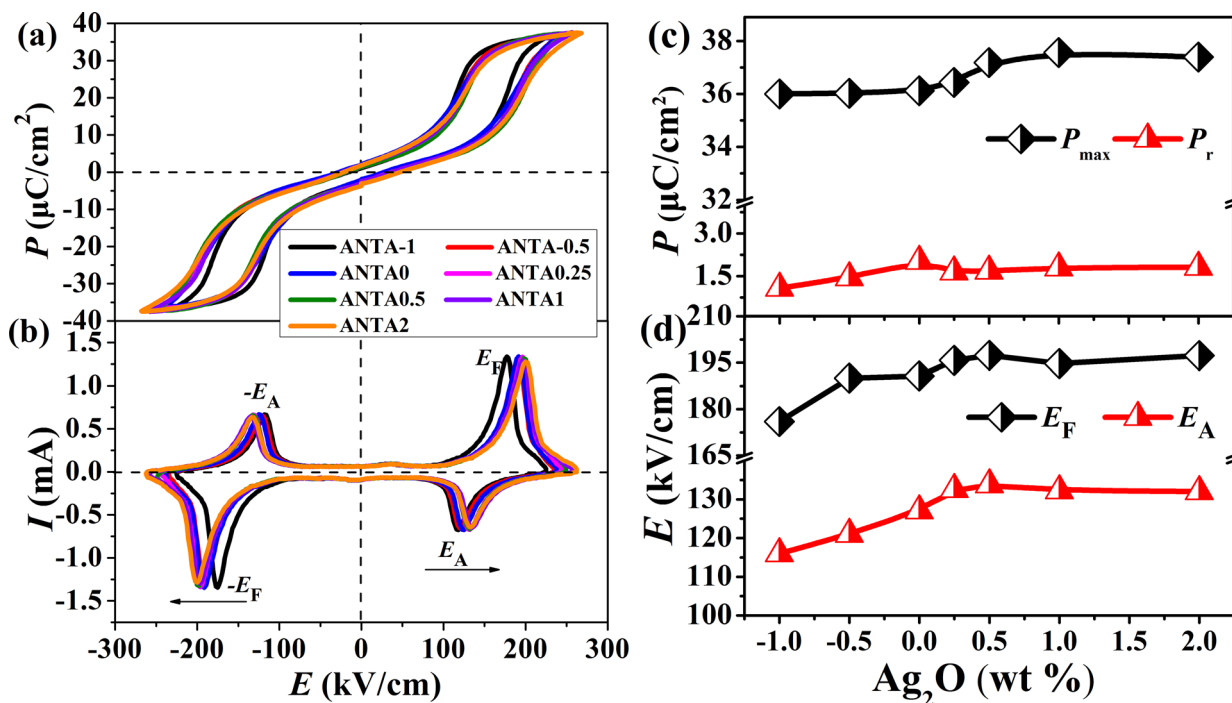


Figure 4: Compositional variation of (a) P - E loops and (b) I - V curves of the as-prepared ANTAx ceramics. The (c) P_{\max} and P_r and (d) E_F and E_A determined from the P - E loops and I - V curves.

The energy storage efficiency:

$$\eta = \frac{W_{\text{rec}}}{W} \times 100\% \quad (6)$$

where E and P are the applied electric field and the dielectric polarization, respectively. Figure 6 gives the as-calculated recoverable energy storage density and efficiency that are obtained from the P - E loops for all as-prepared specimens. The W_{rec} exhibits a general increase with the addition of Ag_2O , with value increasing from 4.0 J/cm^3 for ANTA1 to 4.3 J/cm^3 for ANTA0 ceramics. An obviously increased W_{rec} of 4.8 J/cm^3 is achieved for ANTA1 sample. This demonstrates that a certain of excess Ag_2O is beneficial for improving the recoverable energy storage density. It is worth noting that all ANTAx ceramics exhibit high energy storage efficiency over 68%, which are almost independent on the Ag_2O content, which may be resulted from the synchronous improvement of E_A and E_P . The good energy storage performance demonstrates that the silver stoichiometry engineering is an effective way to improve energy storage density of AgNbO_3 -based antiferroelectric ceramics.

From application viewpoint, the temperature stability of energy storage property should also be considered. To evaluate the effect of silver condition on the reliability of energy storage property, the temperature dependence of P - E loops of ANTA1 ceramics were measured under electric field of 250 kV/cm , as shown in Fig. 7a. The P - E loops are relatively stable with the increase of temperature, exhibiting small variations in both polarization and critical electric field for phase transition. As expected, the ANTA1 ceramics with 1 wt% silver excess demonstrate highly stable energy storage performance in the temperature range from room temperature to $150 \text{ }^\circ\text{C}$, with variations less than 4% and 5% for W_{rec} and η , respectively, as shown in Fig. 7b.

The good energy storage performance further clarifies that the silver stoichiometry-engineered $\text{AgNb}_{0.85}\text{Ta}_{0.15}\text{O}_3$ ceramics are promising for energy storage applications.

Conclusion

In summary, ANTAx lead-free ceramics with various Ag_2O in excess were prepared. The lost silver element during sintering process could be compensated by adding extra 0.5–1 wt% Ag_2O . A small amount of nonstoichiometric Ag_2O played little effect on the phase structure, microstructure, and phase transition temperature, while the critical electric field for antiferroelectric-ferroelectric phase transition and the breakdown strength increased with increasing excess Ag_2O content. As a result, ultrahigh recoverable energy storage density of 4.8 J/cm^3 was achieved for ANTA1 ceramics with 1 wt% Ag_2O in

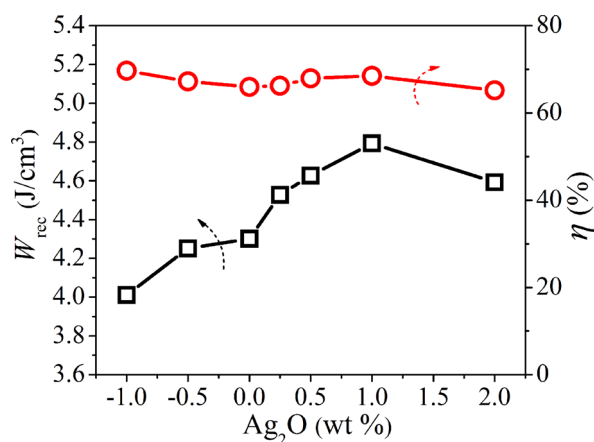


Figure 6: The compositional dependence of energy storage properties (W_{rec} and η) of ANTAx ceramics.

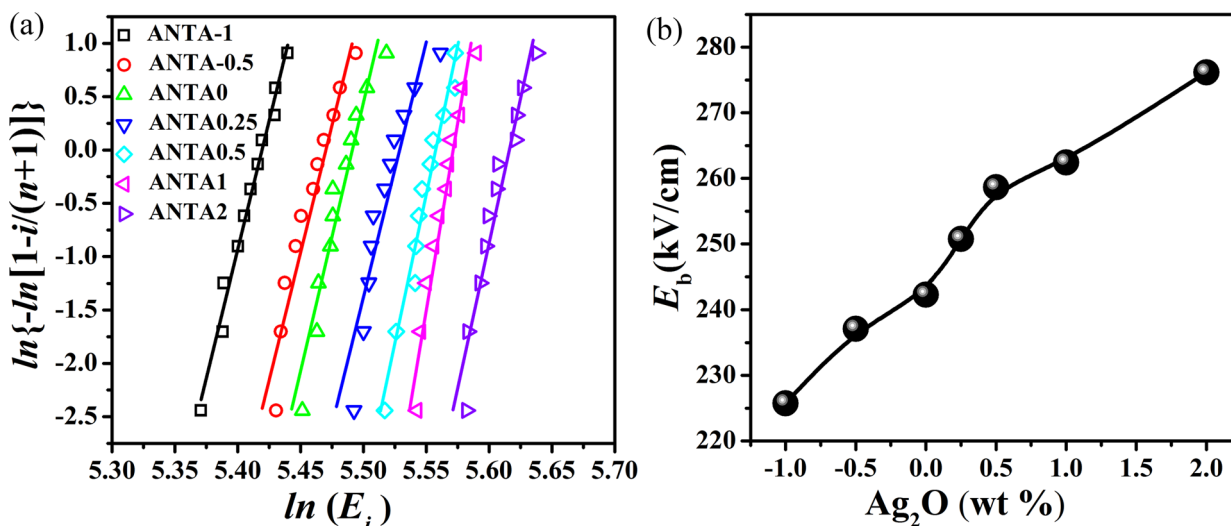


Figure 5: (a) Weibull distribution of breakdown strength. (b) The E_b as a function of Ag_2O content.

excess, demonstrating obvious improvement compared with the stoichiometric counterpart. In addition, the ANTA1 ceramics also exhibited highly stable energy storage performance in the temperature range from room temperature to 150 °C, with variations less than 4% and 5% for W_{rec} and energy storage efficiency, respectively. The good performance indicates that silver stoichiometry engineering is an effective method to improve energy storage properties of AgNbO₃-based antiferroelectric ceramics.

Experimental procedures

The Ag(Nb_{0.85}Ta_{0.15})O_{3-x} wt% Ag₂O (ANTAx) lead-free ceramics with different Ag₂O were prepared by a conventional solid-state reaction method, with the deficient and excess Ag₂O of -1.0 wt%, -0.5 wt%, 0 wt%, 0.25 wt%, 0.5 wt%, 1.0 wt%, and 2.0 wt%. The starting materials were Ag₂O (99.7%), Nb₂O₅ (99.5%), and Ta₂O₅ (99.99%). All raw materials were weighed according to the stoichiometric ratio and ball milled for 24 h in a nylon jar with alcohol as the dispersion medium. After drying, the mixed powders were calcined at 900 °C for 6 h in O₂ atmosphere. Then the as-calcined powders were ball milled and dried again, after which the powders were pressed into green pellets by cold isostatic pressing under pressure of 200 MPa. The pellets were sintered at 1120–1200 °C for 6 h in O₂ atmosphere. The as-sintered samples were polished down to a thickness of ~200 μm and coated with silver electrode (3 mm in diameter) at 560 °C.

The phase structure of the as-sintered samples was determined using X-ray diffractometer (Smartlab-3KW, Rigaku Ltd.,

Tokyo, Japan) with monochromatic Cu Kα radiation, after the ceramics were crushed into powders. The microstructure was observed using a Scanning Electron Microscopy (SEM, Phenom Pro X, Eindhoven, Netherlands), after the as-sintered samples were polished and annealed at temperature slightly lower than their sintering temperature. The metal element content was determined using an inductively coupled plasma atomic emission spectroscopy (ICP-AES, ICPS-7510, Shimadzu, Japan), after the ground sintered ANTAx pellets were dissolved in a H₂SO₄ and HF-mixed solution. The temperature dependence of dielectric permittivity was measured using an LCR analyzer (Model 4294A, Hewlett-Packard Co, Palo Alto, CA, USA) with temperature varying from room temperature to 500 °C. The *P*-*E* loops and the corresponding current vs. electric field (*I*-*E*) curves were measured at 1 Hz with a ferroelectric tester (RT66, Radiant Technologies, NM, USA). The breakdown strength *E*_b was determined using a voltage breakdown tester (RK2671AM, Shenzhen Meiruike electronic technology Co. Ltd, Shenzhen, China).

Acknowledgments

This work is supported by the National Natural Science Foundation of China (Grant No. 52072080, 11864004), the Natural Science Foundation of Guangxi province (Grant No. 2017GXNSFBFA198132), and the Science and Technology Major Project of Guangxi province (Grant No. AA17204100). The author also thanks the fund (Grant No. 20KF-16) from the Key

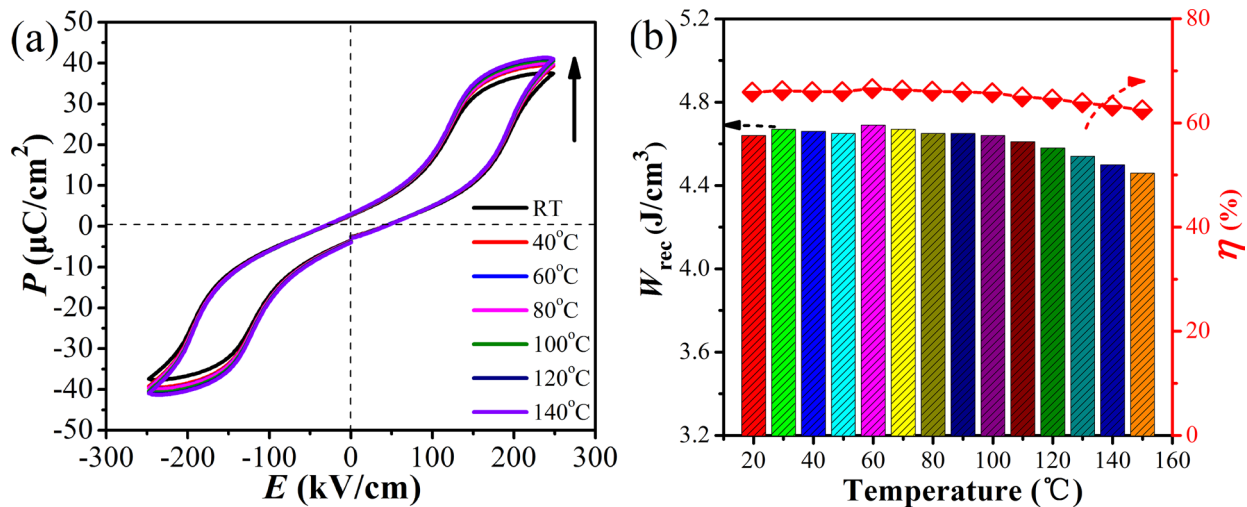


Figure 7: Temperature dependence of (a) *P*-*E* loops and (b) the corresponding energy storage properties of ANTA1 ceramics.

Laboratory of New Processing Technology for Nonferrous Metal & Materials, Ministry of Education/ Guangxi Key Laboratory of Optical and Electronic Materials and Devices, Guilin University of Technology, Guilin (541004), China.

References

- X.H. Hao, A review on the dielectric materials for high energy-storage application. *J. Adv. Dielect.* **3**(01), 1330001 (2013)
- Z. Yao, Z. Song, H. Hao, Z. Yu, M.H. Cao, S.J. Zhang, M.T. Lanagan, H.X. Liu, Homogeneous/Inhomogeneous-Structured Dielectrics and their Energy-Storage Performances. *Adv. Mater.* **29**(20), 1601727 (2017)
- Q. Li, L. Chen, M.R. Gadinski, S.H. Zhang, G.Z. Zhang, H.U. Li, E. Iagodkine, A. Haque, L.Q. Chen, N. Jackson, Q. Wang, Flexible high-temperature dielectric materials from polymer nanocomposites. *Nature* **523**(7562), 576 (2015)
- L.T. Yang, X. Kong, F. Li, H. Hao, Z.X. Cheng, H.X. Liu, J.F. Li, S.J. Zhang, Perovskite Lead-free dielectrics for energy storage applications. *Prog. Mater. Sci.* **102**, 72 (2018)
- H. Zhou, X. Liu, X. Zhu, X. Chen, CaTiO₃ linear dielectric ceramics with greatly enhanced dielectric strength and energy storage density. *J. Am. Ceram. Soc.* **101**(5), 1999 (2018)
- Y. Huang, F. Li, H. Hao, F.Q. Xia, H.X. Liu, S.J. Zhang, (Bi_{0.51}Na_{0.47})TiO₃ based lead free ceramics with high energy density and efficiency. *J. Materiomics.* **5**, 385 (2019)
- Y. Huang, Q.H. Guo, H. Hao, H.X. Liu, S.J. Zhang, Tailoring properties of (Bi_{0.51}Na_{0.47})TiO₃ based dielectrics for energy storage applications. *J. Eur. Ceram. Soc.* **39**(15), 4752 (2019)
- N.N. Luo, K. Han, F.P. Zhuo, L.J. Liu, X.Y. Chen, B.L. Peng, X.P. Wang, Q. Feng, Y.Z. Wei, Design for high energy storage density and temperatureinsensitive lead-free antiferroelectric ceramics. *J. Mater. Chem. C.* **7**, 4999 (2019)
- G.Z. Zhang, D.Y. Zhu, X.S. Zhang, L. Zhang, J.Q. Yi, B. Xie, Y.K. Zeng, Q. Li, Q. Wang, S.L. Jiang, High-energy storage performance of (Pb_{0.87}Ba_{0.1}La_{0.02})(Zr_{0.68}Sn_{0.24}Ti_{0.08})O₃ antiferroelectric ceramics fabricated by the hot-press sintering method. *J. Am. Ceram. Soc.* **98**(4), 1175 (2015)
- Z. Liu, X.F. Chen, W. Peng, C.H. Xu, X.L. Dong, F. Cao, G.S. Wang, Temperature-dependent stability of energy storage properties of Pb_{0.97}La_{0.02}(Zr_{0.58}Sn_{0.335}Ti_{0.085})O₃ antiferroelectric ceramics for pulse power capacitors. *Appl. Phys. Lett.* **106**(26), 262901 (2015)
- Y. Tian, L. Jin, H.F. Zhang, Z. Xu, X.Y. Wei, E.D. Politova, S.Y. Stefanovich, N.V. Tarakina, I. Abrahams, Y.X. Yan, High energy density in silver niobate ceramics. *J. Mater. Chem. A* **4**(44), 17279 (2016)
- L. Zhao, Q. Liu, S.J. Zhang, J.F. Li, Lead-free AgNbO₃ anti-ferroelectric ceramics with an enhanced energy storage performance using MnO₂ modification. *J. Mater. Chem. C.* **4**(36), 8380 (2016)
- N.N. Luo, K. Han, F.P. Zhuo, C. Xu, G.Z. Zhang, L.J. Liu, X.Y. Chen, C.Z. Chen, H.F. Zhou, Y.Z. Wei, Alivalent A-site engineered AgNbO₃ lead-free antiferroelectric ceramics toward superior energy storage density. *J. Mater. Chem. A* **7**(23), 14118 (2019)
- L. Zhao, J. Gao, Q. Liu, S.J. Zhang, J.F. Li, Silver Niobate lead-free antiferroelectric ceramics: enhancing energy storage density by B-site doping. *ACS Appl. Mater. Interfaces* **10**(1), 819 (2018)
- L. Zhao, Q. Liu, J. Gao, S.J. Zhang, J.F. Li, Lead-free antiferroelectric silver niobate tantalate with high energy storage performance. *Adv. Mater.* **29**, 1701824 (2017)
- N.N. Luo, K. Han, M.J. Cabral, X.Z. Liao, S.J. Zhang, C.Z. Liao, G.Z. Zhang, X.Y. Chen, Q. Feng, J.F. Li, Y.Z. Wei, Constructing phase boundary in AgNbO₃ antiferroelectrics: pathway simultaneously achieving high energy density and efficiency. *Nat. Commun.* **11**(1), 4824 (2020)
- K. Han, N.N. Luo, S.F. Mao, F.P. Zhuo, L.J. Liu, B.L. Peng, X.Y. Chen, C.Z. Hu, H.F. Zhou, Y.Z. Wei, Ultrahigh energy-storage density in A-/B-site co-doped AgNbO₃ lead-free antiferroelectric ceramics: insight into the origin of antiferroelectricity. *J. Mater. Chem. A.* **7**(46), 26293 (2019)
- Z.N. Yan, D. Zhang, X.F. Zhou, H. Qi, H. Luo, K.C. Zhou, I. Abrahams, H.X. Yan, Silver niobate based lead-free ceramics with high energy storage density. *J. Mater. Chem. A* **7**(17), 10702 (2019)
- L.Q. Cheng, K. Wang, F.Z. Yao, F.Y. Zhu, J.F. Li, Composition inhomogeneity due to alkaline volatilization in Li-Modified (K, Na)NbO₃ lead-free piezoceramics. *J. Am. Ceram. Soc.* **96**(9), 2693 (2013)
- K. Wang, J.F. Li, Low-temperature sintering of Li-modified (K, Na)NbO₃ lead-free ceramics: sintering behavior, microstructure, and electrical properties. *J. Am. Ceram. Soc.* **93**(4), 1101 (2010)
- N.N. Luo, Q. Li, Z.G. Xia, Effect of Pb(Fe_{1/2}Nb_{1/2})O₃ modification on dielectric and piezoelectric properties of Pb(Mg_{1/3}Nb_{2/3})O₃-PbZr_{0.52}Ti_{0.48}O₃ ceramics. *Mater. Res. Bull.* **46**(9), 1333 (2011)
- N.N. Luo, Q. Li, Z.G. Xia, X.C. Chu, Phase diagram, temperature stability, and electrical properties of (0.85-x)Pb(Mg_{1/3}Nb_{2/3})O₃-0.10Pb(Fe_{1/2}Nb_{1/2})O₃-0.05PbZrO₃-xPbTiO₃ system. *J. Am. Ceram. Soc.* **95**(10), 3246 (2012)
- N.N. Luo, S.J. Zhang, Q. Li, C. Xu, Z.L. Yang, Q.F. Yan, Y.L. Zhang, T.R. Shrout, New Pb(Mg_{1/3}Nb_{2/3})O₃-Pb(In_{1/2}Nb_{1/2})O₃-PbZrO₃-PbTiO₃ quaternary ceramics: morphotropic phase boundary design and electrical properties. *ACS Appl. Mater. Interfaces.* **8**(24), 15506 (2016)
- B.L. Peng, Q. Zhang, X. Li, T.Y. Sun, H.Q. Fan, S.M. Ke, M. Ye, Y. Wang, W. Lu, H.B. Niu, J.F. Scott, X.R. Zeng, H.T. Huang, Giant Electric energy density in epitaxial lead-free thin films with coexistence of ferroelectrics and antiferroelectrics. *Adv. electron. mater.* **1**(5), 1500052 (2015)
- A. Kania, A. Niewiadomski, S. Mig, I. Jankowska-Sumara, M. Pawlik, Z. Ujma, J. Koperski, J. Suchanicz, Silver deficiency and

- excess effects on quality, dielectric properties and phase transitions of AgNbO₃ ceramics. *J. Eur. Ceram. Soc.* **34**(7), 1761 (2014)
26. H.U. Khan, K. Alam, M. Mateenullah, T. Blaschke, B.S. Haq, Synthesis and characterization of solid solution Ag(Nb_xTa_{1-x})O₃ (x = 0, 0.25, 0.5, 0.75, 1.0). *J. Eur. Ceram. Soc.* **35**(10), 2775 (2015)
27. M. Hiroki, C.A.J. Fisher, A. Kuwabara, D.S. Fu, First-principles study of point defect formation in AgNbO₃. *Jpn. J. Appl. Phys.* **52**, 09KF08 (2013)
28. Y. Tian, J. Li, Q.Y. Hu, K. Yu, Y.Y. Zhuang, G. Viola, I. Abrahams, Z. Xu, X.Y. Wei, H.X. Yan, Phase transitions in tantalum-modified silver niobate ceramics for high power energy storage. *J. Mater. Chem. A* **7**(2), 834 (2019)
29. I. Levin, V. Krayzman, J.C. Woicik, J. Karapetrova, T. Proffen, M.G. Tucker, I.M. Reaney, Structural changes underlying the diffuse dielectric response in AgNbO₃. *Phys. Rev. B* **79**(10), 104113 (2009)